$Sr_{1.8}Nd_{1.2}Mn_2O_7$: Synthesis, Crystal Structure, and Physical Properties

P. D. Battle,*,† J. A. Hepburn,† J. E. Millburn,† P. G. Radaelli,‡ M. J. Rosseinsky,*,† L. E. Spring,† and J. F. Vente†

Inorganic Chemistry Laboratory, University of Oxford, South Parks Road, Oxford OX1 3QR, U.K., and Institut Laue-Langevin, P.O. Box 156, 38042 Grenoble Cedex 9, France

Received July 17, 1997. Revised Manuscript Received September 15, 1997[⊗]

A detailed investigation into the preparation of powder samples of the $n = 2$ Ruddlesden−Popper (RP) oxide $Sr_{1.8}Nd_{1.2}Mn_2O_7$ is presented. This material is of interest as it displays colossal magntoresistance (CMR) without three-dimensional ferromagnetic long-range order. It is shown that Rietveld refinement of high-resolution powder X-ray and neutron diffraction data is essential to assess the outcomes of syntheses because of the potential coexistence of two very similar Ruddlesden−Popper phases. Phase coexistence or significant temperature-dependent anisotropic strain can be indicated by the broadening of the {0 0 10} reflection at 5 K. This suggests that a more subtle form of the previously reported phase separation at $x = 0$ is also difficult to avoid at the $x = 0.2$ composition. Precise attention to reaction temperature and time is required to prepare samples containing only one $n = 2$ Ruddlesden−Popper phase, and contamination by small quantities of the $n = \infty$ perovskite is a pervasive problem. Neutron powder diffraction structural analysis of the highest quality sample allows a comparison with the three-dimensional ferromagnet $Sr_{1.8}La_{1.2}Mn_2O_7$. The structure suggests that only slight changes in the Mn−O bond lengths are required to radically alter the electronic structure of $n = 2$ Ruddlesden−Popper phases.

Introduction

Much attention has recently been focused on the $n = 2$ Ruddlesden−Popper (RP) manganates $Sr_{2-x}Ln_{1+x}Mn_2O_7$ due to the observation of colossal magnetoresistance at low applied fields at $x = 0.2$, Ln = La.[1] For Ln = Nd, Pr ($x = 0.0-0.2$), an additional point of interest is that magnetoresistance occurs without any indication of three-dimensional long-range ferromagnetic order in magnetisation measurements.[2,3] The synthesis of bulk single-phase powder samples must avoid intergrowth of other $A_{n+1}B_nO_{3n+1}$ Ruddlesden−Popper homologues such as $n = 1$ K_2NiF_4 and $n = \infty$ perovskite. We recently demonstrated that there is an additional synthesis/characterisation issue to be addressed for these $n = 2$ phases. $Sr_{2-x}Nd_{1+x}Mn_2O_7$ ($x = 0.0, 0.1$)[4] displays phase separation due to the coexistence of two $n = 2$ RP phases with very similar unit-cell volumes. The two phases appear to differ only in the distribution of the Sr^{2+} and Nd^{3+} cations over the two available A cation sites in the $n = 2$ RP structure. This subtle chemical distinction is however sufficient to make the physical properties of the two phases quite different. The phase with the smaller unit-cell volume and a higher strontium concentration on the nine-coordinate rock-salt layer site is an antiferromagnet, while that with the higher strontium concentration on the perovskite site displays a nonzero magnetisation below 250 K, without long-range three-dimensional magnetic order. The magnetic behavior of this second phase is consistent with a description as a spin/cluster glass or two-dimensionally ordered system. These observations require that the phase diagram of this system is worked out in detail, investigating the products of a variety of solid-state reactions using high-resolution diffraction methods. This paper presents the results of such an investigation, focusing on the composition $Sr_{1.8}Nd_{1.2}Mn_2O_7$ which has been claimed to be both single-phase[3] and phase-separated.[5] The focus is on $x = 0.2$ because the jump in the magnetisation at 280 K is most pronounced at this composition in the $Sr_{2-x}Nd_{1+x}Mn_2O_7$ series.[6] The initial focus of the paper is the influence of synthetic conditions on sample quality, assessed with high-resolution variable-temperature powder diffraction data. The structural and magnetic properties of the highest quality sample are then discussed in detail.

Experimental Section

Synthesis and Characterization. Laboratory powder X-ray diffraction data were recorded on both a Philips PW 1410 diffractometer (secondary monochromator, Cu Kα radiation) to monitor the progress of the solid-state reactions discussed below, and a Siemens D5000 powder diffractometer with Cu

† University of Oxford.

‡ Institut Laue-Langevin.

[⊗] Abstract published in *Advance ACS Abstracts,* November 15, 1997.

(1) Morimoto, Y.; Asamitsu, A.; Kuwahara, H.; Tokura, Y. *Nature* **1996**, *380*, 141.

(2) Battle, P. D.; Blundell, S. J.; Green, M. A.; Hayes, W.; Honold, M.; Klehe, A. K.; Laskey, N. S.; Millburn, J. E.; Murphy, L.; Rosseinsky, M. J.; Samarin, N. A.; Singleton, J.; Sluchanko, N. E.; Sullivan, S. P.; Vente, J. F. *J. Phys. Condensed Matter* **1996**, *8*, L427.

(3) Seshadri, R.; Martin, C.; Maignan, A.; Hervieu, M.; Raveau, B.; Rao, C. N. R. *J. Mater. Chem.* **1996**, *6*, 1585−1590.

(4) Battle, P. D.; Green, M. A.; Laskey, N. S.; Millburn, J. E.; Radaelli, P. G.; Rosseinsky, M. J.; Sullivan, S. P.; Vente, J. F. *Phys. Rev. B* **1996**, *54*, 15967.

(5) Battle, P. D.; Green, M. A.; Laskey, N. S.; Millburn, J. E.; Murphy, L. E.; Rosseinsky, M. J.; Sullivan, S. P.; Vente, J. F. *Chem. Mater.* **1997**, *9*, 552.

(6) Battle, P. D.; Green, M. A.; Laskey, N. S.; Millburn, J. E.; Rosseinsky, M. J.; Spring, L. E.; Sullivan, S. P.; Vente, J. F. *J. Mater. Chem.* **1997**, *7*, 977.

S0897-4756(97)00512-7 CCC: $14.00 © 1997 American Chemical Society

$K\alpha_1$ radiation for Rietveld analysis. Sample quality during synthesis was monitored by scans of the {0 0 10} reflection of the $n = 2$ RP phase on the D5000 instrument. The difference in c lattice parameter between the coexisting Ruddlesden−Popper phases makes the width of this reflection very sensitive to sample quality: broadening can only be indicative of inhomogeneity or phase separation as a lowering of the crystal symmetry cannot split this reflection. The instrumental resolution of the D5000 in the angular range of the {0 0 10} reflection is 0.076° 2θ ($\Delta d/d = 1.5 \times 10^{-3}$).

For two samples, high-resolution powder X-ray diffraction data were recorded at room temperature on station 2.3 at the Daresbury Synchrotron Radiation Source at a wavelength of 1.399 Å (determined using a silicon standard), in Bragg−Brentano geometry with a resolution in the vicinity of {0 0 10} of 0.047° 2θ ($\Delta d/d = 1 \times 10^{-3}$).

Powder neutron diffraction data for precise crystal structure refinement and phase analysis were recorded on two high-resolution diffractometers. Measurements on the time-of-flight neutron powder diffractometer HRPD at the ISIS spallation source, Rutherford Appleton Laboratory, U.K. used the 1 m sample position with a $\Delta d/d$ resolution of 8×10^{-4}, which is constant across the diffraction pattern. The constant wavelength D2B instrument at the Institut Laue-Langevin, Grenoble was operated in its high intensity mode at $\lambda = 1.5942$ Å (for Rietveld refinement, the highest resolution in this mode is $\Delta d/d = 1.1 \times 10^{-3}$ at $2\theta = 136°$) and 2.3979 Å (for higher Q-resolution measurement of the {0 0 10} reflection with $\Delta d/d = 2.2 \times 10^{-3}$, compared with 4.4×10^{-3} when measuring this reflection with 1.59 Å radiation). Data were collected at room temperature and at 5 K. Rietveld profile refinement was carried out using the CCSL[7] and GSAS[8] program suites.

Neutron powder diffraction data at longer d spacings were collected to search for magnetic scattering, on the IRIS time-of-flight diffractometer at ISIS over the range $1 \leq d/\text{Å} \leq 7.4$ and on the D1B constant wavelength diffractometer (ILL, $\lambda = 2.52$ Å).

Magnetic measurements were made using a Quantum Design MPMS SQUID magnetometer on 20 mg samples contained in gelatin capsules.

Compounds were prepared by solid state reaction between dried Nd_2O_3, $SrCO_3$, and MnO_2 in alumina crucibles. Both subsolidus reactions and the use of a volatile Bi_2O_3 flux[3] were investigated. Samples were studied by high-resolution and laboratory powder diffraction at several points during the reaction. Chemical analysis (ICP AES) indicated that the products had the desired compositions with respect to the constituent metals.

Subsolidus Reaction. The starting materials (5 g) were thoroughly ground and fired at 800 °C (1 day), 1000 °C (1 day), 1200 °C (1 day), and 1300 °C (3 × 1 day) with grinding and repelletizing (13 mm diameter pellets) carried out at each stage. Powder X-ray diffraction showed that all the starting materials had reacted after the third firing at 1300 °C. X-ray data were collected on the D5000 instrument for Rietveld analysis at this stage (sample **A**). The sample was then split into three parts, which were subjected to different thermal treatments. A 0.3 g 8 mm diameter pellet was prepared and heated in air at 1500 °C for 18 h, followed by diffraction characterization on the D5000 and on station 2.3 at the SRS (**B**). An identical thermal treatment was applied to a 2 g batch of 8 mm diameter pellets (**C**). This sample was characterized by time-of-flight neutron powder diffraction on HRPD at RAL. Finally, the remaining 2 g of **A** was pressed into 8 mm diameter pellets and subjected to an 18 h 1500 °C treatment. This was combined with **C** and fired at 1500 °C for a further 4 h to yield sample **D**. Following laboratory diffraction characterisation, powder neutron diffraction data were collected on sample **D** on the D2B (298, 5 K) and D1B powder diffractometers (1.5, 50, and 150 K).

(7) David, W. I. F.; Ibberson, R. M.; Matthewman, J. Rutherford Appleton Laboratory Report RAL-92-032, 1992.

(8) Larson, A. C.; Von Dreele, R. B. *General Structure Analysis System*; Los Alamos National Laboratory, 1994.

Table 1. Cell Parameters and Phase Fractions for the Two $n = 2$ Ruddlesden−Popper Phases in Sample A of $Sr_{1.8}Nd_{1.2}Mn_2O_7$ (1300 °C Reaction Temperature, 3 days)[a]

	a/Å	c/Å	V/Å^3	fraction/%
phase 1	3.8426(1)	20.1067(9)	296.90(2)	46(2)
phase 2	3.8412(1)	20.1369(8)	297.13(2)	54(2)

[a] The fractions presented here and in subsequent tables are mole fractions.

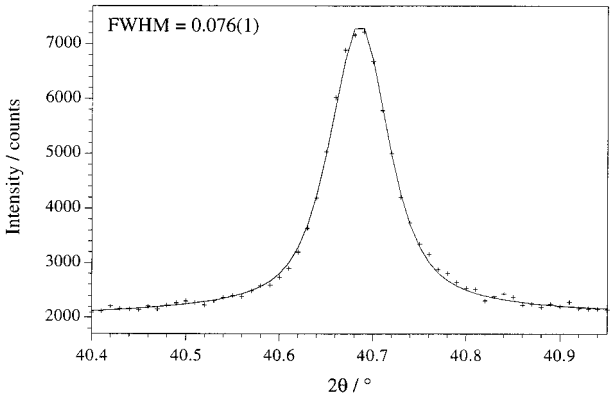

Figure 1. Fit of a pseudo-Voigt function to the {0 0 10} reflection of sample **B** of $Sr_{1.8}Nd_{1.2}Mn_2O_7$ (measured on station 2.3 of the Daresbury SRS).

Flux Route. Sample **E** was prepared on an identical scale and with the same firing sequence as reported in ref 3. Sample **F** was a 5 g sample which required an extra 19 h at 1500 °C to remove impurity peaks and sharpen the broad {0 0 10} reflection observed on the D5000 diffractometer after the initial reaction. This sample was studied on the HRPD (298, 5 K) and IRIS (2, 50, and 298 K) neutron powder diffractometers. Following the collection of neutron data, the effect of extended annealing at the synthesis temperature of 1500 °C was investigated by heating **F** for a further 5 days at this temperature.

Results

Ambient-Temperature X-ray Characterization during Synthesis. The 0.148(6)° width and peak shape of the {0 0 10} reflection measured on the D5000 instrument indicated that the subsolidus sample after the initial 1300 °C reaction sequence (**A**) was inhomogeneous, consistent with the phase separation and strain arguments presented later. The lattice parameters, unit-cell volumes, and phase fractions derived from the X-ray Rietveld refinement of this sample are given in Table 1. The outcome of the subsequent heat treatments shows that the sample size and reaction temperature all play a role in determining sample quality.

The 1500 °C treatment of the small pellet (**B**) reduced the width of the {0 0 10} reflection to 0.096(6)°, approaching the resolution limit of the D5000 instrument. The width of this reflection when measured on station 2.3 was 0.076(1)°, with a very good fit to a single pseudo-Voigt profile (Figure 1).

The larger 2 g batch given the same thermal treatment (**C**) displayed greater differential and total broadening of the {0 0 10} reflection on the D5000 instrument, the width of 0.109(7)° being 0.02° broader than the neighboring {1 1 6} reflection. The subsequent 4 h reaction time at 1500 °C (**D**) reduced the {0 0 10} width to 0.088(6)°, compared to 0.080(2)° for the neighboring {1 1 6} reflection.

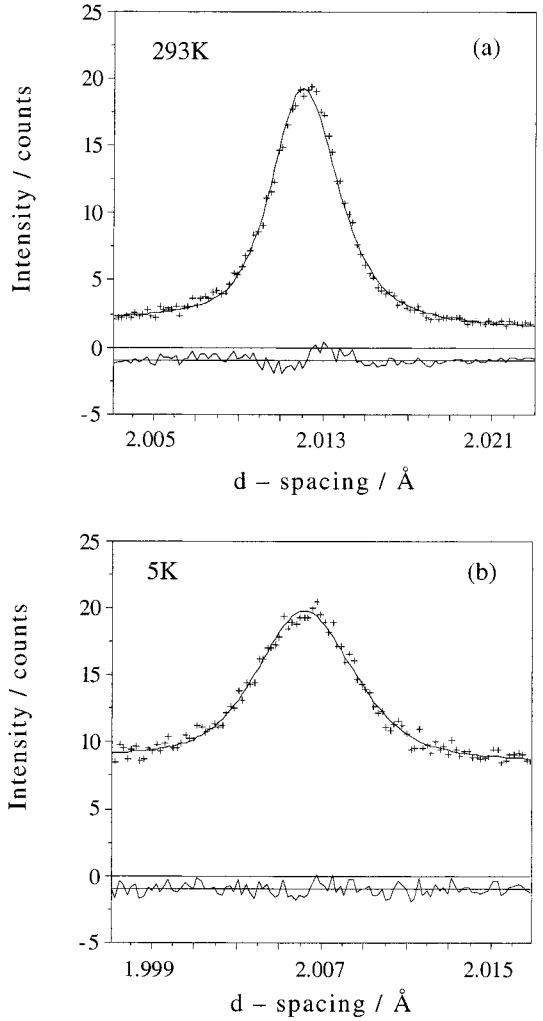

Figure 2. {0 0 10} reflection of sample **C** of $Sr_{1.8}Nd_{1.2}Mn_2O_7$ measured on HRPD (a) at 293 K (b) at 5 K, showing the broadening observed on cooling. The fit shown is to a pseudo-Voigt function convoluted with double-exponential decay.

The small flux-derived sample **E** has a {0 0 10} width of 0.104(2)° when measured on station 2.3 at the SRS, and 0.138(2)° on the D5000. The further 36 h 1500 °C anneal of **F**, which had a {0 0 10} width of 0.125(4)° on the D5000, produced substantial decomposition into the $n = \infty$ perovskite phase.

High-Resolution Powder Neutron Diffraction and Crystal Structure Refinements. Sample **C** was studied at 5, 50, and 298 K on the HRPD diffractometer. The {0 0 10} reflection cannot be satisfactorily fitted in a conventional single-phase Rietveld refinement, even when incorporating excess broadening for $l \neq 0$ reflections ($\chi^2 = 2.7$ at 5 K) and broadens significantly on cooling from $\Delta d = 0.0031$ Å at 293 K to 0.0053 Å at 5 K (Figure 2). Two more complex refinement strategies produce similar, satisfactory results. The SAPS (sample and peak shape) code allows refinement of separate Lorentzian and Gaussian peak shape parameters for every reflection in the pattern,[9] consistent with the assumption that the excess broadening of the {0 0 10} arises from a distribution of anisotropic strains within a single-phase sample, and giving $\chi^2 = 1.6$ (101 variable parameters). A model with two Ruddlesden−Popper phases gives $\chi^2 = 1.4$ (47 variable parameters, Figure 3). The improvement over the conventional single phase refinement from the above two models is greater at 5 and 50 K than at room temperature. Lattice parameters, phase fractions and the Mn−O bond lengths for 5 and 293 K are given in Table 2. The 5 and 293 K HRPD data for **F** are similar, although the {0 0 10} reflection is broader at room temperature.

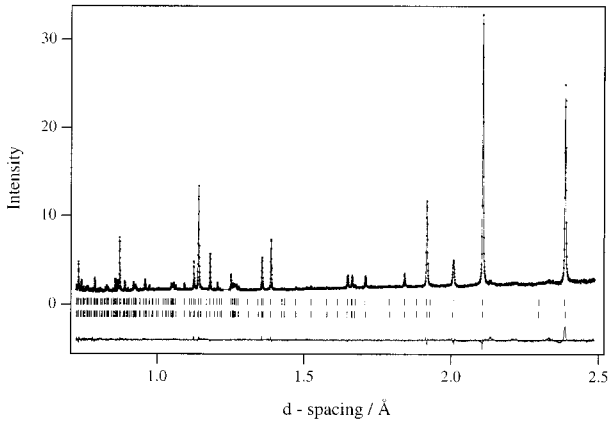

Figure 3. Two-phase Rietveld refinement of sample **C** of $Sr_{1.8}Nd_{1.2}Mn_2O_7$ at 5 K (time-of-flight neutron powder diffraction on HRPD). The observed data are crosses, the calculated model is a solid line, and the difference is given below. The ticks mark the positions of the Bragg reflections from the two phases.

Table 2. Parameters Derived from a Two-Phase $n = 2$ RP Rietveld Refinement of Time-of-Flight Powder Neutron Diffraction Data on $Sr_{1.8}Nd_{1.2}Mn_2O_7$ (Sample C) at 5 and 293 K[a]

	phase 1 (293 K)	phase 2 (293 K)	phase 1 (5 K)	phase 1 (5 K)
a/Å	3.84031(5)	3.83901(6)	3.83631(8)	3.83321(8)
c/Å	20.1307(3)	20.1464(4)	20.0626(7)	20.0904(6)
V/Å^3	269.887(8)	269.917(8)	295.269(6)	295.199(6)
fraction/%	54	46	54(2)	46(2)
Mn−O(1)/Å	1.956(11)	1.938(9)	1.911(11)	1.965(10)
Mn−O(2)/Å	2.060(12)	2.035(12)	2.077(14)	2.021(13)
Mn−O(3)/Å	1.92016(5)	1.91955(9)	1.9191(4)	1.9169(2)

[a] The weight fractions of the two phases in the 293 K refinement were fixed at the 5 K values. $\chi^2 = 2.8$, $R_w = 6.24\%$ (293 K). $\chi^2 = 1.96$, $R_w = 2.81\%$ (5 K).

The D2B data collected on sample **D** do not show a pronounced broadening of the {0 0 10} width on cooling, although the resolution in the vicinity of the {0 0 10} reflection is lower than that of HRPD. The width measured at 1.59 Å on D2B was $\Delta d/d = 4.5 \times 10^{-3}$ at both temperatures, compared with an instrumental resolution of 4.4×10^{-3} in this angular range. The higher resolution data collected at 2.4 Å at 5 K are well-fit by a single pseudo-Voigt peak with a Δd width of 0.0069(6) Å, slightly broader than the neighboring {1 1 6} reflection ($\Delta d = 0.0064(2)$ Å). Rietveld refinement of the 1.59 Å data at both 5 and 298 K was satisfactory using only a *single* $n = 2$ Ruddlesden−Popper phase plus a small quantity of $n = \infty$ perovskite second phase, with *Imma* space group symmetry and unit-cell volume consistent with the structure of $Nd_{0.5}Sr_{0.5}MnO_3$.[10] In this case, there was *no* significant improvement in the fit when a second $n = 2$ RP phase was added to the refinement ($\chi^2 = 1.80$ for 3 phases at 298 K, 4.43 at 5

(9) David, W. I. F.; Akporiaye, D. E.; Ibberson, R. M.; Wilson, C. C. Rutherford Appleton Laboratory Report RAL-88-103, 1988.

(10) Caignaert, V.; Millange, F.; Hervieu, M.; Suard, E.; Raveau, B. *Solid State Commun.* **1996**, *99*, 173.

Table 3. Parameters Derived from Combined Refinement of Powder X-ray and Neutron (D2B) Data of Sample D of $Sr_{1.8}Nd_{1.2}Mn_2O_7$ at 298 K[a]

	z	U_{iso} (Å^2)	U_{11} (Å^2)	U_{22} (Å^2)	U_{33} (Å^2)
Sr/Nd(1)[b]	1/2	0.0031(4)			
Sr/Nd(2)[c]	0.31752(6)	0.0037(3)			
Mn	0.0972(1)	0.0023(3)			
O(1)	0	0.017[d]	0.0248(9)	0.0248(9)	0.001(1)
O(2)	0.19789(9)	0.020[d]	0.0169(8)	0.0169(8)	0.026(1)
O(3)	0.09723(6)	0.010[d]	0.0102(5)	0.0026(5)	0.0172(5)

[a] The refined parameters of the majority phase were insensitive to any composition change due to the presence of the perovskite impurity. The atoms were refined at the following positions in the unit cell: Sr/Nd(1) 2b 0 0 1/2: Sr/Nd(2), O(2) and Mn 4e 0 0 *z*: O(1) 2a 0 0 0: O(3) 8 g 0 1/2 *z*. $a = 3.83999(7)$ Å, $c = 20.1457(4)$ Å, $V = 297.06(2)$ Å^3. $R_F = 3.8\%$ (neutrons) 11.7% (X-rays). *Imma* perovskite nominally $Nd_{0.5}Sr_{0.5}MnO_3$ 2.82(2) wt %. $a = 5.438(6)$ Å, $b = 7.715(1)$ Å, $c = 5.4001(7)$ Å, $V = 226.60(4)$ Å^3. Agreement indexes: neutrons ($10 \le 2\theta/° \le 149.5$): $R_{wp} = 4.84\%$, $R_p = 3.75\%$, DWd = 0.80. X-rays ($15 \le 2\theta/° \le 115$): $R_{wp} = 6.89\%$, $R_p = 5.47\%$, DWd = 1.68. Totals: $R_{wp} = 5.55\%$, $R_p = 4.85\%$, DWd = 1.21, $\chi_{red}^2 = 1.66$ for 55 variables. A pseudo-Voigt peak-shape function (X-ray GW, LY, asymmetry: neutron GU, GV, GW, LX, LY, asymmetry) and an eight-term shifted Chebyshev polynomial background function were used in each histogram. The neutron wavelength was refined to be 1.59362(3) Å. [b] Nd content 34(1)%. [c] Nd content 43.0(7)%. [d] The U_{iso} value quoted for O(1)−O(3) is the equivalent isotropic displacement parameter.

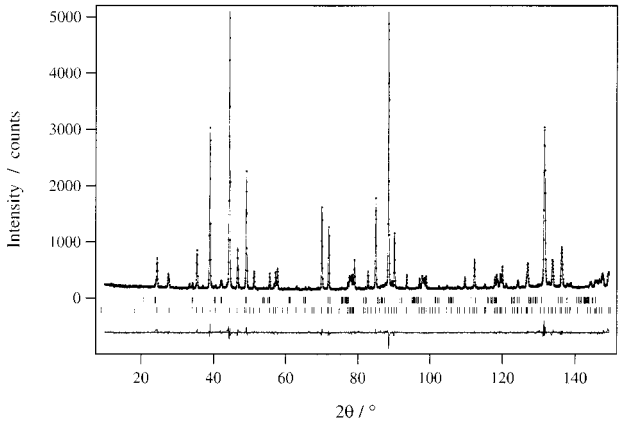

Figure 4. Rietveld refinement of sample **D** (D2B constant wavelength neutron data, $\lambda = 1.59$ Å) of $Sr_{1.8}Nd_{1.2}Mn_2O_7$ at 298 K, presented as in Figure 3. The upper set of tick marks correspond to the Bragg reflections from the minority *Imma* $n = \infty$ perovskite.

K) and anisotropic broadening of the $l \neq 0$ reflections was not required in the analysis. This is consistent with the {0 0 10} width of **D** at room temperature on the D5000, which is the narrowest of all the samples studied. All the figures of merit thus indicate that sample **D** is the closest to a truly single-phase bulk sample of this composition which we have been able to prepare. We therefore present the results of the Rietveld refinement of this sample in detail, although we emphasize that our measurements do not exclude the possibility of temperature-dependent broadening of the {0 0 10} reflection of **D**: they simply demonstrate that any such effect is too small to be seen on the diffractometers used.

The room-temperature structure of sample **D** was determined using combined refinement of D5000 X-ray and D2B constant wavelength neutron powder diffraction histograms. (Table 3 and Figure 4) χ^2 fell from 1.76 when anisotropic displacement parameters were employed for the oxide anions. The structure at 5 K was refined from 1.59 Å neutron data alone, with a similar

Table 4. Parameters Derived from Refinement of Powder Neutron (D2B) Data of Sample D of $Sr_{1.8}Nd_{1.2}Mn_2O_7$ at 5 K[a]

	z	U_{iso} (Å^2)	U_{11} (Å^2)	U_{22} (Å^2)	U_{33} (Å^2)
Sr/Nd(1)[b]	1/2	−0.0028(6)			
Sr/Nd(2)[c]	0.31792(8)	0.0015(4)			
Mn	0.0970(2)	−0.0014(6)			
O(1)	0	0.0164[d]	0.024(1)	0.024(1)	0.00(1)
O(2)	0.1976(1)	0.0154[d]	0.011(1)	0.011(1)	0.023(2)
O(3)	0.09754(8)	0.0072[d]	0.0026(7)	0.0016(7)	0.0172(8)

[a] $a = 3.83572(5)$ Å, $c = 20.0855(4)$ Å, $V = 295.51(2)$ Å^3. Agreement indexes: neutrons: $R_{wp} = 5.55\%$, $R_p = 4.15\%$, $R_F = 3.89\%$, DWd = 0.62. $\chi_{red}^2 = 3.96$ for 40 variables. Perovskite as second phase: *Imma* 3.2(2) wt%; $a = 5.4310(7)$ Å, $b = 7.711(2)$ Å, $c = 5.397(1)$ Å, $V = 226.05(5)$ Å^3. [b] Nd content fixed at 34%. [c] Nd content fixed at 43%. [d] The U_{iso} value quoted for O(1)−O(3) is the equivalent isotropic displacement parameter.

Table 5. Bond Lengths (Å) and Angles (deg) Derived from 298 and 5 K Rietveld Refinements of Sample D of $Sr_{1.8}Nd_{1.2}Mn_2O_7$

		298 K	5 K
Mn−O(1)	(1×)	1.958(2)	1.948(4)
Mn−O(2)	(1×)	2.029(3)	2.021(5)
Mn−O(3)	(4×)	1.92000(4)	1.91789(4)
Mn−Mn (*z*,-*z*)		3.916(4)	3.896(8)
Sr/Nd(1)−O(1)	(4×)	2.71528(5)	2.71227(4)
Sr/Nd(1)−O(3)	(8×)	2.7429(9)	2.741(1)
Sr/Nd(2)−O(2)	(1×)	2.410(2)	2.417(3)
Sr/Nd(2)−O(2)	(4×)	2.7330(2)	2.7301(4)
Sr/Nd(2)−O(3)	(4×)	2.576(1)	2.561(2)
O(1)−Mn−O(3)		90.03(8)	90.3(1)
Mn−O(3)−Mn[a]		179.960(1)	179.342(3)

[a] This angle is equal to the O(3)−Mn−O(3) angle by symmetry.

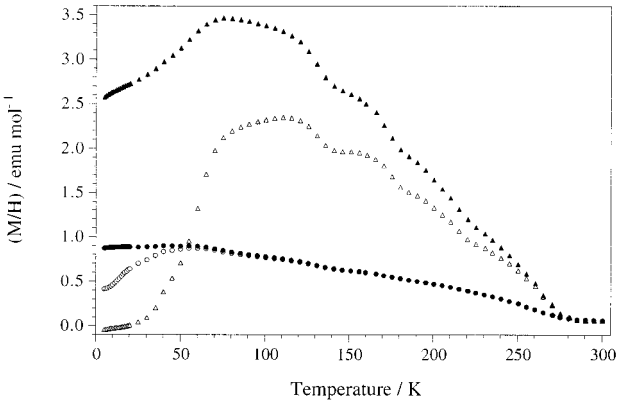

Figure 5. Magnetization measurements on sample **D** of $Sr_{1.8}Nd_{1.2}Mn_2O_7$ in 0.01 T (triangles) and 0.1 T (circles) fields. The full symbols represent field-cooled (FC) data, empty symbols represent zero-field-cooled (ZFC) data.

improvement on the introduction of anisotropic displacement parameters. The small negative values of the displacement parameters for Sr/Nd(1) and Mn reflect the reduced thermal motion of these ions at 5 K combined with absorption effects (Tables 4 and 5).

Search for Magnetic Scattering in $Sr_{1.8}Nd_{1.2}Mn_2O_7$. Magnetization measurements on sample **D** (Figure 5) are similar, though not identical, to those presented earlier on this composition.[3,6] The increase in magnetization at 280 K is followed by a nonmonotonic temperature dependence which indicates several possible magnetic phase transitions and guided the choice of data collection temperatures in the neutron powder diffraction experiments. The zero magnetization below 20 K in the 0.01 T zero-field-cooled (ZFC) measurement indicates that all the spins in the sample are involved

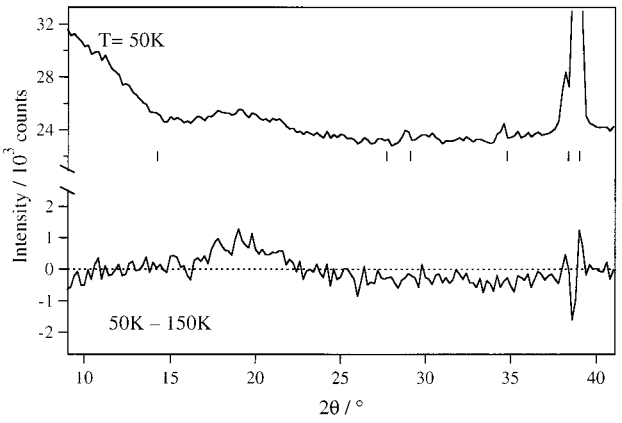

Figure 6. Normalized difference between the D1B neutron powder diffraction datasets collected on sample **D** of $Sr_{1.8}Nd_{1.2}Mn_2O_7$ at 50 and 150 K. (The data at 150 K have been subtracted from those at 50 K.) The tick marks indicate the positions of the nuclear Bragg reflections from the $n = 2$ RP phase.

in cooperative magnetism, with no pure paramagnetic response.

Neither samples **D** (measured on D1B) nor **F** (IRIS) showed magnetic Bragg peaks in the neutron diffraction patterns at any temperature. The quality of the fit to the nuclear Bragg reflections to either sample is unaffected at 5 K, indicating the absence of ferromagnetic long-range order: the maximum ferromagnetic moment consistent with the data is 0.5 μ_B per Mn.

Inspection of data collected at 50, 150, and 300 K on sample **D** on D1B do indicate the onset of magnetic short-range order, however. Figure 6 is the normalized difference between the datasets collected at 50 and 150 K, and the broad distribution of excess scattering in the 17−22° angular range can be ascribed to the development of correlated regions of spins at low temperature. The absence of a marked decrease in the lower angle paramagnetic scattering suggests that this is dominated by the Nd^{3+} moments at both temperatures.

Discussion

High-resolution powder diffraction data from $Sr_{1.8}Nd_{1.2}Mn_2O_7$ shows that $l \neq 0$ reflections are subject to temperature-dependent anisotropic broadening. Satisfactory refinement of these data requires the use of a generalized anisotropic strain model, in which the mechanism producing the strain is itself temperature dependent, or refinement with two discrete Ruddlesden−Popper phases of differing cell dimensions. For sample **C**, the biphasic model produced a slightly superior fit to the HRPD data. In either case, the inhomogeneity can be assigned to fluctuations in the distribution of Sr and Nd over the two distinct sites in the Ruddlesden−Popper structure within a unit cell once the mean Sr/Nd ratio has become homogeneous across all the unit cells throughout the sample.[4] The difference between the two models is that the composition distribution shows two distinct maxima in the biphasic case but is a broad Gaussian with a single mean in the anisotropic strain model. Failure to fit the {0 0 10} reflection to a single peak is a clear indication of the existence of two discrete phases, while excess broadening compared to other classes of reflection, as observed for example for **C** here, is consistent with either model. High synthesis temperatures favor the formation of single phases, explaining the relatively large site-to-site fluctuations found in our original $x = 0.2$ sample prepared at 1300 °C.[5] These fluctuations appear to become less severe as the neodymium concentration increases. The difference between the two phases refined for sample **C** is much less marked than found for $x = 0.0$ and $x = 0.1$, e.g., the mean Mn−O bond lengths and unit-cell volumes differ by a factor of 10 less than found previously. The biphasic model has the advantage that the temperature dependence of the diffraction pattern is readily explicable in terms of the differing thermal expansion of the two phases. Temperature dependent local strains in an inhomogeneous but single-phase sample can also be ascribed to anisotropic local variations in lattice parameter with temperature producing increased broadening on cooling. In view of the local electronic differences implied by either of these models, attention to details of sample characterization during synthesis is particularly important here.

The extent of the {0 0 10} broadening can be controlled by sample size, annealing time, and annealing temperature. A useful figure of merit for sample quality is that a {0 0 10} width of greater than 0.10° on the D5000 or the 2.3 diffractometers corresponds to multiple $n = 2$ RP phase behavior or significant anisotropic strain broadening. Extended high-temperature annealing, to minimize the inhomogeneity in the Sr/Nd distribution over the two sites in the $n = 2$ phase by facilitating cation diffusion, encounters the competing problem of decomposition, possibly via the formation of intergrowth-rich intermediates, into the $n = \infty$ perovskite which is evidently more thermodynamically stable. The synthetic procedure used to prepare sample **D** is the best we have been able to devise, using the criteria discussed above, and we therefore discuss the structure refinement of this sample in detail. An ORTEP representation of the structure is given in Figure 7.

The individual Mn environment is quite distorted, consistent with the 4*mm* site symmetry, as the bonds to the axial oxygens Mn−O(1) (joining the bilayers) and Mn−O(2) (in the rock salt layer) are longer (by 0.04 and 0.1 Å, respectively) than the equatorial Mn−O(3) bonds connecting the octahedra within the planes. The extent of this distortion is slightly reduced on cooling: the dimensionless parameter $(r_{ax} - r_{eq})/(r_{ax} + r_{eq})$ is 0.0189(6) at 298 K and 0.017(1) at 5 K, where r_{ax} is taken as the mean values of the axial bond lengths. The distortion is more pronounced as the manganese oxidation state is reduced toward +III, by comparison with both the antiferromagnetic and spin-glass phases in the biphasic $x = 0.0$ and $x = 0.1$ samples.[4] This is consistent with an increasing concentration of Jahn−Teller active Mn^{III} centers.

The A cation ordering revealed by the ambient X-ray plus neutron refinement is consistent with previous X-ray studies.[3,5] The Sr fraction on the perovskite site is slightly but significantly greater (66(1)%) than the value corresponding to a random distribution (60%) while the rock-salt layer site (56.9(7)%) is slightly deficient in strontium.

The oxygen atomic displacement parameters measured at 5 K are similar in size to those found at room temperature, indicating that local disorder makes an

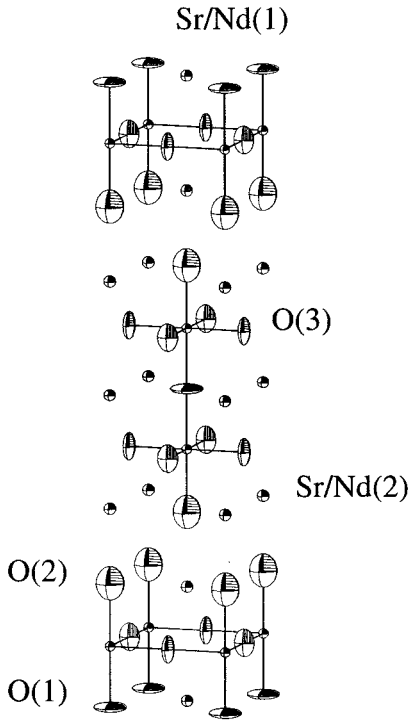

Figure 7. ORTEP representation of the structure of $Sr_{1.8}Nd_{1.2}Mn_2O_7$ (sample **D**) at 298 K, determined by combined refinement of X-ray and neutron histograms. Atoms are represented as 90% thermal ellipsoids.

important contribution to their size. Inspection of the anisotropic thermal ellipsoids of the oxygen anions (Figure 7) indicates that those within the bilayer are as expected, being elongated perpendicular to the Mn−O bonds. The ellipsoid of O(2), in the rock-salt layer, is elongated along the Mn−O(2) bond. This is suggestive of static positional disorder due to the presence of both Jahn−Teller Mn^{III} and non-Jahn−Teller Mn^{IV} centers. The position of O(2) will also be sensitive to the presence of both Sr^{2+} and Nd^{3+} on the rock-salt site, because the distance between Sr/Nd(2) and O(2) is the closest A cation−oxide contact. The root-mean-square O(2) displacement of 0.16 Å (0.12 Å at 5 K) is comparable with the difference in Shannon−Prewitt ionic radius of 0.13 Å between Sr^{2+} and Nd^{3+}, suggesting that the position of O(2) can respond locally to whether the nearest-neighbor Sr/Nd(2) site is occupied by Sr^{2+} or Nd^{3+}. The similarity of the oxide displacement parameters at 298 and 5 K is also relevant to the bilayer geometry: the two-dimensional sheets of corner sharing octahedra are on average completely flat within error at room temperature and only buckle by 0.6° at 5 K, but the extent of static disorder suggests that uncorrelated local corrugation may be significant.

The above detailed picture of the structure of $Sr_{1.8}Nd_{1.2}Mn_2O_7$ can be used to explain the pronounced differences between the effect of La^{3+} and Nd^{3+} as counterions in the $n = 2$ RP phases. The antiferromagnetism observed for both $Sr_{2.04}La_{0.96}Mn_2O_7$ and $Sr_2NdMn_2O_7$ is suppressed with increasing Mn^{III} concentration,[11] but $Sr_{1.8}La_{1.2}Mn_2O_7$ is a conventional ferromagnet with a moment of 3.0 μ_B/Mn and a transition temperature of 126 K.[1] In the Nd^{3+} case, the absence of magnetic Bragg scattering from $Sr_{1.8}Nd_{1.2}Mn_2O_7$ shows that the increased Mn^{III} concentration is insufficient to produce ferromagnetic long-range order here. The departure from octahedral regularity is larger in $Sr_{1.8}Nd_{1.2}Mn_2O_7$, which becomes *less* distorted on cooling, than in $Sr_{1.8}La_{1.2}Mn_2O_7$ ($(r_{ax} - r_{eq})/(r_{ax} + r_{eq}) =$ 0.0078 (298 K) and 0.0091 (5 K) for the La^{3+} analogue[12])- where the distortion increases below the metal−insulator transition at 126 K. The enhanced distortion of the MnO_6 octahedra in the Nd^{3+} phase has been associated with an enhanced extent of Jahn−Teller distortion and consequent e_g electron localization.[3] Double exchange, a dominant ferromagnetic contribution to the exchange interactions in metallic manganates, is then suppressed, leaving only +III − +IV e_g superexchange to compete with the antiferromagnetic t_{2g}−t_{2g} interactions.

The appearance of diffuse scattering at low temperature is consistent with the development of regions of correlated spins within the sample. The idea that these magnetic correlations are ferromagnetic and two-dimensional is consistent with recent single-crystal studies on compounds in the $La_{2-x}Sr_{1+x}Mn_2O_7$ series[13,14] which indicate two-dimensional ordering near room temperature. The in-plane Mn−O(3) bonds are shorter in the Nd^{3+} case while both the Mn−O(1) and Mn−O(2) axial bonds are longer. This reduces the coupling between bilayers and also between the two layers comprising a bilayer, thereby increasing the two-dimensionality of the structure from an electronic point of view. The exchange interaction between the bilayers is via the Mn−O(2) bond, which is 0.035 Å longer in $Sr_{1.8}Nd_{1.2}Mn_2O_7$ than in $Sr_{1.8}La_{1.2}Mn_2O_7$. This increase in length may be due to the increased occupancy (43% vs 33% La^{3+} in $Sr_{1.8}La_{1.2}Mn_2O_7$[3,5]) of the rock salt site by the Nd^{3+} cation (which is smaller and more acidic than La^{3+}), together with enhanced localization of the e_g electrons. The rise in the magnetization of $Sr_{1.8}Nd_{1.2}Mn_2O_7$ below 280 K can then be attributed to formation of small ferromagnetic clusters of spins, possibly within the perovskite bilayers to give a two-dimensionality correlated system. The absence of three-dimensional order therefore results from reduced interbilayer coupling in the neodymium compound. In this picture, the high two-dimensional ordering/cluster formation temperatures are indicative of the intrablock ferromagnetic correlations being comparable to those found in the three-dimensional $Nd_{1-x}Sr_xMnO_3$ perovskites. This may be attributed to a larger concentration of Sr^{2+} per Ln^{3+} at a given oxidation state in the $n = 2$ structure, reducing the mean acidity of the A cation site and thus its competition for covalency with oxygen.

Conclusion

The above high-resolution neutron power diffraction studies show that inhomogeneous ordering of Sr^{2+} and Nd^{3+} over the rock-salt and perovskite sites is a persistent problem in the synthesis of $Sr_{2-x}Nd_{1+x}Mn_2O_7$ phases. In our hands, samples with one $n = 2$ RP phase

(11) Battle, P. D.; Cox, D. E.; Green, M. A.; Millburn, J. E.; Radaelli, P. G.; Rosseinsky, M. J.; Spring, L. E.; Vente, J. F. *Chem. Mater.* **1997**, *9*, 1042.

(12) Mitchell, J. F.; Argyriou, D. N.; Jorgensen, J. D.; Hinks, D. G.; Potter, C. D.; Bader, S. D. *Phys. Rev. B* **1997**, *55*, 63.

(13) Argyriou, D. N.; Mitchell, J. F.; Potter, C. D.; Bader, S. D.; Kleb, R.; Jorgensen, J. D. *Phys. Rev. B* **1997**, *55*, 11965.

(14) Kimura, T.; Tomioka, Y.; Kuwahara, H.; Asamitsu, A.; Tamura, M.; Tokura, Y. *Science* **1996**, *274*, 1698.

contain a small amount of $n = \infty$ perovskite impurity, suggesting competition between increased Sr/Nd order and formation of thermodynamically stable products as cation diffusion becomes easier. The increased neodymium concentration makes the problem less severe at $x = 0.2$ than for $x = 0.0$ and 0.1, and neither phase in biphasic samples of $x = 0.2$ orders magnetically. The absence of three-dimensional ferromagnetism in comparison with $Sr_{1.8}La_{1.2}Mn_2O_7$ suggests that magnetic long-range order is controlled by the axial bond lengths around manganese: increased distortion leads to a reduction in the extent of coupling between the bilayers. In view of the low-field magnetoresistance ascribed to interlayer coupling in $n = 2$ RP phases,[14] the substantial effect of such a small structural change is both surprising and significant.

Acknowledgment. We thank the EPSRC and the donors of the Petroleum Research Fund, administered by the American Chemical Society, for their support of this work. We thank Dr. R. M. Ibberson (ISIS) and Dr. C. C. Tang (Daresbury Laboratory) for their assistance with the collection of the neutron time-of-flight and synchrotron powder diffraction data.

CM970512L